ACS APPLIED MATERIALS & INTERFACES

Research Article

www.acsami.org

Stable Core/Shell CdTe/Mn-CdS Quantum Dots Sensitized Three-Dimensional, Macroporous ZnO Nanosheet Photoelectrode and Their Photoelectrochemical Properties

Weili Li, Pengtao Sheng, Hongyan Feng, Xuehua Yin, Xuewei Zhu, Xu Yang, and Qingyun Cai*

State Key Lab of Chemo/Biosensing & Chemometrics, College of Chemistry & Chemical Engineering, Hunan University, Changsha 410082, China

Supporting Information

ABSTRACT: A novel photoelectrode based on ZnS/CdTe/Mn-CdS/ZnS-sensitized three-dimensional macroporous ZnO nanosheet (NS) has been prepared by electrodeposition and successive ion layer adsorption and reaction (SILAR) method. The photoelectrode performances were significantly improved through the coupling of the core/shell CdTe/Mn-CdS quantum dots (QDs) with ZnO NS, and the introduction of the ZnS layer as a potential barrier. The photocurrent density systematically increases from ZnO NS (0.45 mA/cm^2), CdTe/Mn-CdS/ZnO NS (4.98 mA/cm^2), to ZnS/CdTe/Mn-CdS/ZnS/ZnO (6.23 mA/cm^2) under the irradiation of AM 1.5G simulated sunlight. More important, the ZnS/CdTe/Mn-CdS/ZnS-sensitized ZnO NS photoelectrode provides a remarkable photoelectrochemical cell efficiency of 4.20% at −0.39 V vs Ag/AgCl.

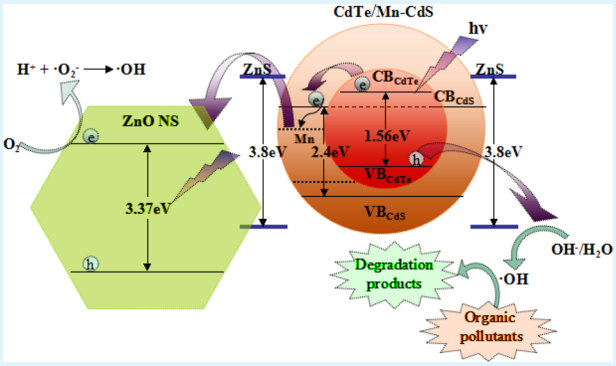

KEYWORDS: *SILAR, photoelectrochemical, quantum dots, macroporous ZnO nanosheet, photocatalytic degradation*

INTRODUCTION

In recent years, ZnO has been widely investigated as a promising alternative photoanode material for photoelectrochemical cell.[1,2] This trend can be attributed to the fact that ZnO has much higher electron diffusivity than that of TiO_2.[3,4] Moreover, various ZnO nanostructures such as zero-dimensional, one-dimensional (nanowire), two-dimensional (nanosheets), and three-dimensional (multilayer porous nanosheets) can grow directly on transparent substrates through low-cost and simple chemical routes, giving a wide direct band gap of 3.37 eV and large exciton binding energy of 60 m eV. To increase the light-harvesting efficiency, various semiconductor nanocrystals including CdS,[5−7] CdSe,[8,9] and CdTe[10] have been adopted to sensitize ZnO. For example, Singh et al.[5] reported the fabrication of ZnO nanoparticles for CdS quantum dots-sensitized solar cell. Yong et al.[7] prepared a novel ZnO/CdS core/shell nanowire heterostructure array for the potential applications in nanowire-based photoelectrochemical cells. Dam et al.[9] demonstrated that CdS and CdSe-cosensitized three-dimensional porous ZnO nanosheet photoelectrodes could be potentially useful materials in light-harvesting applications. Jiang et al.[10] encapsulated thickness-tunable CdTe quantum dots shell onto ZnO nanorod arrays forming an intact interface. More interestingly, Li et al.[11] designed novel double-sided CdS and CdSe quantum dots cosensitized ZnO nanowires for photoelectrochemical hydrogen generation. According to previous reports,[12] fabrication of photoelectrodes with the help of one-dimensional nanostructures,[7,8,10] which can provide a direct rather than zigzag pathway for electron transfer as compared to zero-dimensional nanoparticle analogues,[5] has proven to be an effective way to facilitate electron transport. However, insufficient internal surface area of nanowires limits the conversion efficiency at a relatively low level due to the limited sensitizer loading. In contrast, three-dimensional macroporous ZnO NS[6,9] not only can offer a large specific surface area for the deposition of sensitizers but also facilitate the diffusion of electrolyte.[13] More importantly, the macroporous ZnO NS in situ grown on conducting substrate is also expected to afford more excellent electron transfer comparable to nanowires.[6] Studies show that cosensitizing ZnO with different nanocrystals[9,10] such as CdSe/CdTe,[14] CdS/CdTe,[15] and CdS/CdSe[16] can extend the light absorption to the infrared range, and more importantly align the energy bands of the semiconductor. Ho et al.[17] utilized ZnO nanowire/nanoparticles composite films as photoanodes to cosensitize CdS/CdSe/ZnS. Cao et al.[18] reported a bilayer photoelectrode constructed by ZnO nanoparticle and ZnO microsphere scattering layer for CdS/CdSe QD cosensitized solar cells. Unfortunately, macroporous ZnO NS substrate has not been used in cosensitized strategy. Here, we choose macroporous ZnO NS as substrate to load cosensitizers. Among the different

Received: April 9, 2014
Accepted: July 10, 2014
Published: July 10, 2014

   dx.doi.org/10.1021/am502151m | ACS Appl. Mater. Interfaces 2014, 6, 12353−12362

QD compositions, we are particularly interested in CdTe QDs, a p-type semiconductor possessing a large absorption coefficient with a direct band gap of E_g = 1.56 eV.[19] Further, the conduction band energy of CdTe is favorable for electron injection into ZnO.[10] As compared to single composition QDs, QDs with core/shell nanoheterostructure are superior in that the relative positions of the conduction band and valence bands of the two components can be chosen to tailor the electron and hole distributions to control the single and multiple exciton lifetimes. On the basis of this consideration, core/shell CdTe/Mn-CdS QDs were chosen to extend the light-harvesting ability of ZnO NS into the visible region in this work. Synthesis of Mn doped II−VI semiconductor and their photophysical properties has been the subject of recent reports.[21,22] Using Mn-CdS QDs as the shell has been proven to be a powerful strategy to extend the lifetime of charge carriers to boost the efficiency.[23] So far, to our knowledge, this is the first report to apply Mn-doping shell in the CdTe/Mn-CdS core−shell system. To further improve the CdTe/Mn-CdS/ZnO NS photolelctrode performances, ZnS shell was introduced as a dual-function potential barrier to reduce the leakage of electrons on intefaces, which has been demonstrated to be an efficient interface treating strategy for performance improvement.[24,25] An overall conversion efficiency of 4.2% was observed in the ZnS/CdTe/Mn-CdS/ZnS/ZnO NS photoelectrode.

EXPERIMENTAL SECTION

Preparation of Three-Dimensional, Macroporous ZnO NS. Zinc nitrate hexahydrate ($Zn(NO_3)_2{\cdot}6H_2O$), mercaptoacetic acid (MAA), terephthalic acid (TA), manganese acetate ($Mn(CH_3COO)_2$), Na_2TeO_3, $NaBH_4$, $Cd(NO_3)_2$, Na_2S, and Na_2SO_3 of analytical reagent grade were purchased from commercial sources and used as supplied. The ZnO NS was electrodeposited onto FTO glass substrate in an aqueous electrolyte containing 0.05 M $Zn(NO_3)_2{\cdot}6H_2O$ and 0.1 M KCl using an electrochemical workstation.[26] The electrodeposition was performed at −1.0 V for 30 min at 70 °C. Prior to electrodeposition, the FTO substrate was cleaned ultrasonically for 10 min in acetone, 10 min in ethanol, and then rinsed with distilled water. The as-synthesized ZnO NS was sintered at 450 °C for 30 min in air atmosphere to obtain macroporous structure. To recycle the FTO, the used substrate was immersed into so-called piranha solution (1:3 of 30% H_2O_2:H_2SO_4) for 30 min, then rinsed with distilled water several times to reuse.

Preparation of CdTe QDs and CdTe/ZnO NS Photoelectrode. Water-soluble MAA capped CdTe QDs were synthesized according to our previously reported method.[20] First, 40 mg of MAA was added to 100 mL of ultrapure water containing 91.5 mg of cadmium acetate under nitrogen atmosphere. Next, 0.5 M NaOH was used to adjust the pH to 8.5. Under constant bubbling, 175.5 mg of trisodium citrate and 17.9 mg of Na_2TeO_3 were added in sequence. Last, 10.5 mg of $NaBH_4$ was added. Note that bubbling was kept on another 30 min until all of the insolubles disappeared. Finally, the above solution was placed in a high-pressure reaction kettle, and kept boiling at 120 °C for 5 min. The obtained CdTe QDs capped with MAA were directly absorbed onto the ZnO NS by immersing the ZnO NS in a CdTe QD aqueous solution at 25 °C for 12 h.

Fabrication of ZnS/CdTe/Mn-CdS/ZnS/ZnO NS Photoelectrode. SILAR was used to coat CdTe/ZnO NS with CdS shell. The free MAA molecules in CdTe QDs aqueous solution can capture Cd^{2+} to form core/shell CdTe/CdS QDs during the coating step. Briefly, CdTe/ZnO NS substrate was successively soaked 30 s in 0.05 M $Cd(NO_3)_2$ aqueous solutions and 30 s in 0.05 M Na_2S aqueous solutions. This step was repeated nine times to obtain CdS shell. For CdS or Mn-CdS-modified ZnO NS photoelectrodes preparation, this step is repeated five times. The Mn-CdS shell coated CdTe/ZnO NS photoelectrodes were prepared with similar methods (nine layers), but with 0.05 M $Cd(NO_3)_2$ containing 0.0375 M $Mn(CH_3COO)_2$ as cation source.[23] This allowed coadsorption of Mn^{2+} and Cd^{2+} ions. The ZnS buffer layer was prepared according to previous literature.[14,25] For ZnS pretreatment, 0.05 M $Zn(NO_3)_2$ in ethanol and 0.05 M Na_2S in methanol/water (7:3, v/v) were used for one SILAR process with a dipping time of 1 min for each cycle and repeated for 15 cycles. For ZnS post-treatment, we dipped the sensitized photoelectrode two times in 0.1 M $Zn(NO_3)_2$ and 0.1 M Na_2S aqueous solutions 1 min for each dipping.

Photoelectrochemical Measurements and Apparatus. All electrodeposition and electrochemical measurements were performed with a CHI electrochemical analyzer (CHI660C, Shanghai Chenhua Instrument Co. Ltd.) using a conventional three-electrode system comprised of a Ag/AgCl reference electrode, working electrode, and a Pt sheet counter electrode containing 0.35 M Na_2SO_3 and 0.24 M Na_2S (pH = 11.5). The incident light from a 300 W Xe lamp was filtered to match the AM 1.5G spectrum with an intensity of 88 mW/cm^2 as measured by a radiometer (OPHIR, Littleton, CO).

Scanning electron microscopy (SEM, JSM-6700F), high-resolution transmission electron microscopy (HRTEM), and transmission electron microscopy (TEM, JEOL, JEM 2100) were used to character the morphology and dimension of the products. Energy dispersive X-ray spectrometers (EDS) fitted to the HRTEM were used for elemental analysis. Photoluminescence spectra (PL) and absorption spectra were recorded by a F-4600 fluorescence spectrophotometer (Hitachi, Japan) and Cary 300 (Agilent, U.S.), respectively. Brunauer−Emmett−Teller (BET) surface area was measured by BELSORP-MINI II 00668.

Photocatalytic Degradation of 2,4-Dichlorophenoxyacetic Acid (2,4-D) and Anthracene-9-carboxylic Acid (9-AnCOOH). The photoelectrocatalytic degradation of organic pollutants was carried out in 0.05 M Na_2SO_4 electrolyte under AM 1.5G illumination in a cubic quartz reactor containing 20 mL of 2,4-D or 9-AnCOOH at an initial concentration of 20 mg/L. The concentration change during the degradation procedure was monitored by determining the UV−visible adsorption of 50 μL of sample taken from the solution. After measurement, the solution was immediately added back to the reaction cell to keep the volume constant.

Analysis of Photodegradation Mechanism. Hydroxyl radicals (·OH) produced by the as-prepared photoelectrode under AM 1.5G illumination were detected by the PL analysis using TA as probe molecule.[27] Experimental steps are similar to those of the degradation procedure except that organic pollutant solution is replaced by the 5×10^{-4} M TA and 2×10^{-3} M NaOH. The change of ·OH concentration during the degradation procedure was monitored by determining the fluorescence emission intensity with an excitation wavelength of 320 nm.

RESULTS AND DISCUSSION

Characterization of the Cosensitized Materials. Supporting Information Figure S1 shows the SEM images of $Zn_5(OH)_8Cl_2{\cdot}H_2O$ (A,B, without crystallization) and ZnO NS (C,D, with crystallization). Supporting Information Figure S1B and D shows the corresponding high-resolution images of (A) and (C), respectively. After crystallization at 450 °C for 30 min, the morphology of nanosheet turns from smooth surface (Supporting Information Figure S1A and B) into three-dimensional macroporous structure with the same sheetlike hexagon (Supporting Information Figure S1C and D) with edge length of 1.5−3 μm and thickness of 300−400 nm. As we know, the nanosheet obtained from electrodeposition consists of $Zn_5(OH)_8Cl_2{\cdot}H_2O$ crystals.[26] After crystallization, the smooth surface turned into macroporous structure resulting from the pyrolysis of $Zn_5(OH)_8Cl_2{\cdot}H_2O$. To evaluate the porous structure, nitrogen adsorption and desorption measurements were performed. The corresponding isotherms are shown in Supporting Information Figure S2. The BET surface area of the hierarchically ZnO NS was 17.8 m^2/g, which is much bigger than that of the ZnO powder (<3 m^2/g)[28] or single layer porous ZnO NS (9.56 m^2/g).[29] The large specific surface area was attributed to the macroporous structure embedded in three-dimensional

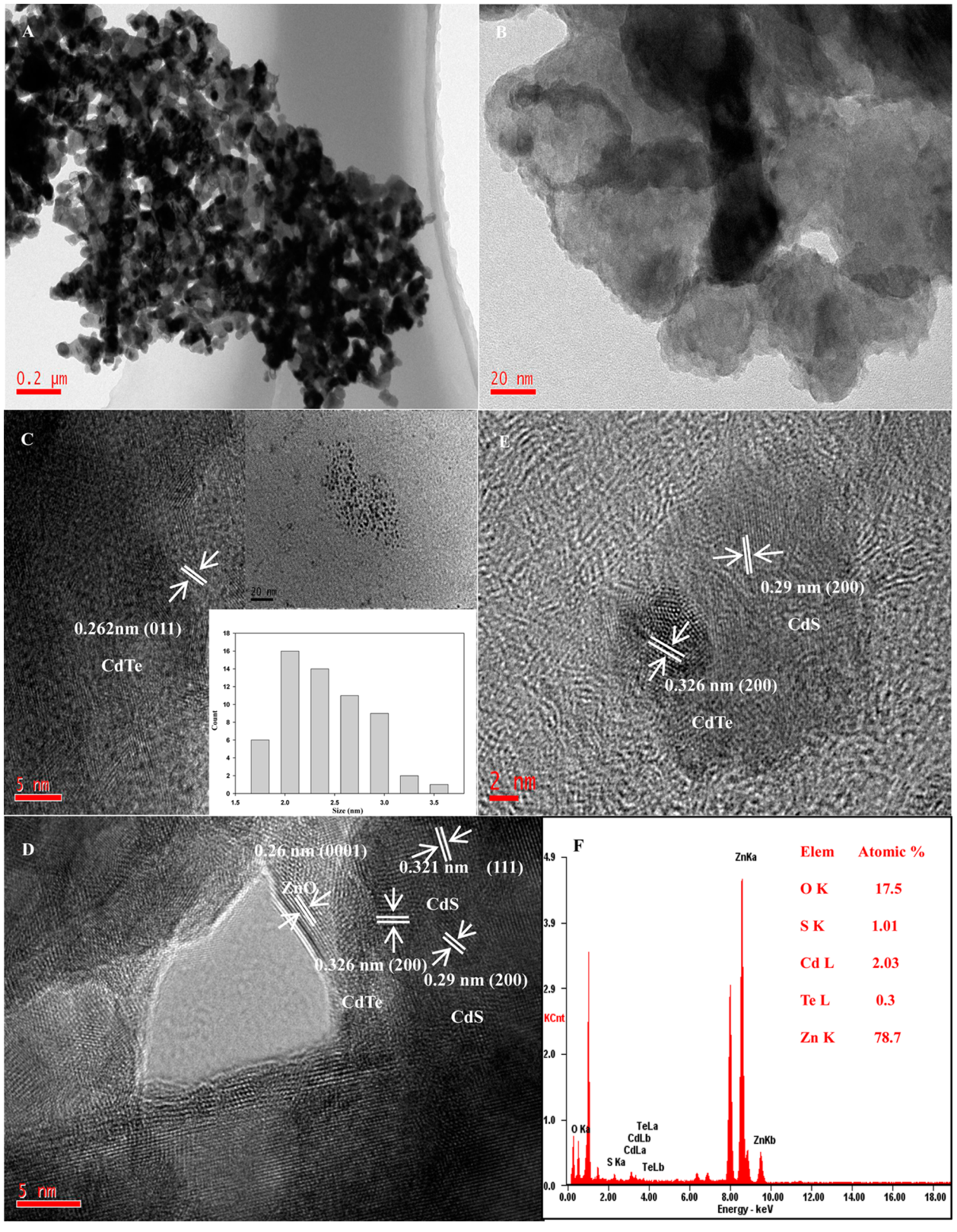

Figure 1. TEM images of CdTe/CdS/ZnO NS with different magnification (A,B). HRTEM images of CdTe QDs-modified ZnO NS (C), CdTe/CdS/ZnO NS (D), and core/shell CdTe/CdS QDs (E). (F) shows the EDS spectrum of CdTe/CdS/ZnO NS. Morphology and the sizes histogram of the as-prepared CdTe QDs are shown in the inset of (C).

microarchitectures, which will benefit the following deposition of QDs sensitizers.

The TEM image of the cosensitized CdTe/CdS/ZnO NS is shown in Figure 1A. The corresponding high-resolution image of Figure 1B clearly displays that the naked ZnO NS surface is fully covered with sensitizers. These closely packed sensitizers would benefit the carriers transport without space barriers. It is noted that the deposition of the sensitizers does not obviously change

dx.doi.org/10.1021/am502151m | ACS Appl. Mater. Interfaces 2014, 6, 12353−12362

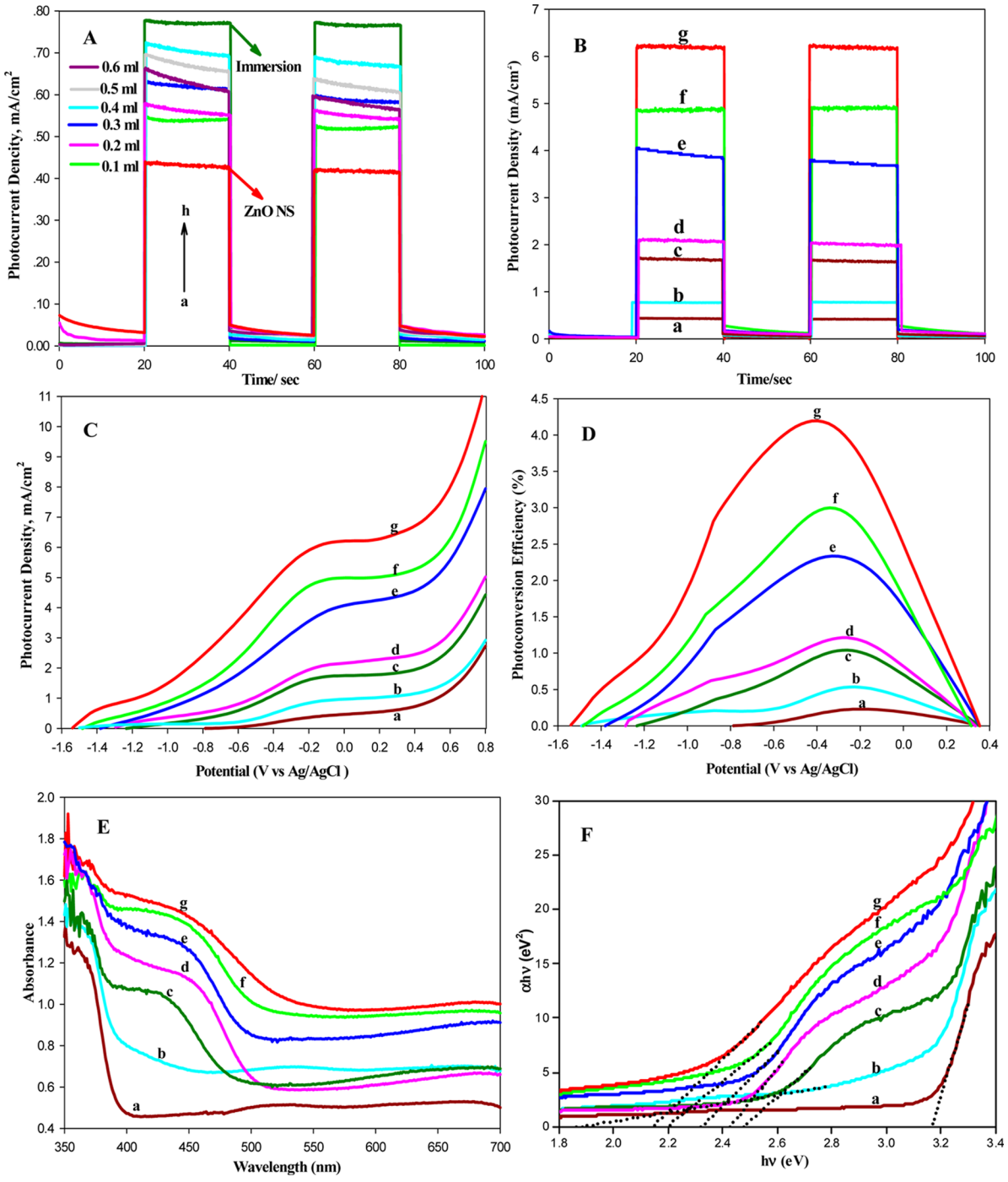

Figure 2. (A) The light on/off photocurrent responses of CdTe/ZnO NS in which CdTe QDs were immobilized by immersing the ZnO NS in CdTe QD solution (curve h) or dropping 0.1−0.6 mL of CdTe QDs solution onto ZnO NS (curves b−g). (B,C) The photocurrent responses and $J-V$ characteristics measured under AM 1.5G illumination of 88 mW/cm^2 sunlight. (D) Photoconversion efficiency corresponding to (C). (E) UV−vis absorption spectra, and (F) $(\alpha h\nu)^2$ versus $h\nu$ plot for determining the absorption onset of different photoelectrodes. For all curves of (B)−(F): a, ZnO NS; b, CdTe QDs/ZnO NS; c, CdS/ZnO NS; d, Mn-CdS/ZnO NS; e, core/shelnl CdTe/CdS/ZnO NS; f, core/shell CdTe/Mn-CdS/ZnO NS; g, ZnS/CdTe/Mn-CdS/ZnS/ZnO NS.

the macroporous morphology of ZnO NS. This is very important for the incident light absorption even within the thick nanosheet, which results in excellent photoelectrochemistry performance. To prepare the cosensitized photoelectrode, pure ZnO NS should be first modified with CdTe QDs by immersing it into a CdTe QD solution. Figure 1C shows the HRTEM image of CdTe QDs-modified ZnO NS. One can see that the CdTe QDs are uniformly deposited onto the ZnO NS surface. The lattice spacing measured is 0.262 nm corresponding to the (011) plane of the CdTe QDs (JPCDS 41-0941).[19] The insets of Figure 1C display the spherical morphology of CdTe QDs and the corresponding size histogram with an average diameter of 2.4 nm. Such size CdTe QDs show the maximum photocurrent response according to our previous report.[20] HRTEM image of Figure 1D reveals the core/shell structure of CdTe/CdS on the ZnO NS. The lattice spacing of 0.26 nm corresponds to ZnO Ns

on which the CdTe QDs surrounded by CdS are anchored. The lattice spacing of 0.326 nm corresponds to the (200) plane of the CdTe QDs (JCPDS 65-0880), and those of 0.29 and 0.321 nm correspond to the (200) and (111) planes of the CdS shell (well-matched to the reference data JCPDS 80-0019), respectively.[7] Here, the CdS shell has a polycrystalline structure, and is closely contacted with both the CdTe QDs and the ZnO NS, forming a novel core/shell structure assembled onto the ZnO NS surface. The core−shell structure of CdTe/CdS was further confirmed by the HRTEM image of Figure 1E, which clearly depicts that CdTe with a lattice spacing of 0.326 nm is encapsulated by CdS with a lattice spacing of 0.29 nm. The EDS spectrum shown in Figure 1F reveals the characteristic peaks of O, S, Cd, Te, and Zn.

Optimization of the Photoelectrodes. CdTe QDs were first immobilized on ZnO NS by either dropping 0.1−0.6 mL of CdTe QD solution on the ZnO NS or immersing the ZnO NS in this CdTe QD solution. Although the photocurrent density increases from 0.54 to 0.65 mA/cm^2 with increasing dropped solution from 0.1 to 0.6 mL (Figure 2A, curves b−g), the immersion method gives a higher photocurrent density of 0.77 mA/cm^2 than the dropping method probably due to the more efficient loading of CdTe QDs (Figure 2A, curve h). The naked ZnO NS is with a photocurrent density of 0.45 mA/cm^2 (Figure 2A, curve a).

Further immobilization of CdS or Mn-CdS QDs on the CdTe QDs-immobilized ZnO NS resulted in dramatic increases of the photocurrent up to 4.06 or 4.98 mA/cm^2 by nine SILAR cycles. Overloading of CdS or Mn-CdS QDs beyond nine SILAR cycles formed a loose particle-packing film resulting in decreases in photocurrents because such a loose network structure was with a lot of grain boundaries, which acted as both recombination centers and potential barrier to block the transport of carriers between adjacent crystals. The dramatic increases in photocurrent are the results of synergetic effects of these materials because the photocurrent densities of CdS or Mn-CdS QDs-immobilized ZnO NS were only 1.71 or 2.07 mA/cm^2 (Figure 2B, curves c,d).

Photoelectrochemical Behavior Evaluation. Figure 2C shows the $J-V$ (current density versus potential) curves for ZnO NS with different modifications measured with 88 mW/cm^2 AM 1.5G illumination. The light to chemical energy conversion efficiencies shown in Figure 2D are calculated as follows:[11]

$$\eta\ (\%) = [(\text{total power output} - \text{electrical power input})/\text{light power input}] \times 100$$

$$= j_p[E^0_{\text{rev}} - |E_{\text{RHE}}|]/I_0 \times 100$$

where j_p is the photocurrent density (mA/cm^2) shown in Figure 2C, E^0_{rev} is the standard reversible potential (1.23 V/NHE), I_0 is the power density of incident light (88 mW/cm^2), and E_{RHE} is the applied voltage versus reversible hydrogen electrode (RHE) calculated from the measured potentials ($E_{\text{Ag/AgCl}}$) versus the Ag/AgCl reference electrode via the Nernst equation:

$$E_{\text{REH}} = E_{\text{Ag/AgCl}} + 0.059\text{pH} + E^{\circ}_{\text{Ag/AgCl}}$$

where $E^{\circ}_{\text{Ag/AgCl}}$ is the standard potential of Ag/AgCl at 25 °C (0.1976 V). In this work, pH = 11.5, therefore $E_{\text{REH}} = E_{\text{Ag/AgCl}} + 0.8761$.

The photocurrent density over the investigated potential range follows an increasing trend according to naked ZnO NS, CdTe/ZnO NS, CdS/ZnO NS, Mn-CdS/ZnO NS, core/shell CdTe/CdS/ZnO NS, core/shell CdTe/Mn-CdS/ZnO NS, and ZnS/CdTe/Mn-CdS/ZnS/ZnO NS. The photoresponse is related to both the light absorption ability and the composite structure. Figure 2E shows the UV−vis absorption spectra of these photoelectrodes. Because both CdTe and CdS are direct-band gap semiconductor,[19,30] their absorption coefficients are related to the excitation energy ($E_{\text{exc}} = h\nu$) by $(\alpha h\nu)^2 = \text{const} - (h\nu - E_g)$,[30] where E_g is the band gap energy. To obtain the absorption onset, $(\alpha h\nu)^2$ is plotted against energy $h\nu$ shown together with UV−vis absorption spectra in Figure 2F. Extrapolation of the linear part until its intersection with the $h\nu$ axis gives the values of E_g. As shown in Figure 2E, the naked ZnO NS absorbs only UV light (less than 390 nm) due to its large band gap of 3.17 eV (curve a, Figure 2E). Incorporation of CdTe QDs onto ZnO NS extends the absorption spectrum significantly into the visible region (curve b, Figure 2E) with absorption edge approximately at 660 nm corresponding to a bandgap of 1.87 eV (curve b, Figure 2F), which match well with the reported value.[31] The absorption spectra of CdS/ZnO NS show absorption onset around 500 nm corresponding to a bandgap of 2.48 eV (curve c, Figure 2F). Interestingly, the absorption spectrum of the Mn-CdS/ZnO NS (curve d, Figure 2E) resembles that of CdS/ZnO NS except with higher absorbance and an obvious red-shift with absorption onset around 512 nm corresponding to a bandgap of 2.42 eV (curve d, Figure 2F). The absorption of the core/shell CdTe/CdS/ZnO NS is further red-shifted with absorption onset at ∼532 nm (curve e, Figure 2E) corresponding to a band gap of 2.33 eV (curve e, Figure 2F), which displays a complementary and enhancement effect in the light harvest as compared to the single sensitizer. Replacing CdS with Mn-CdS shell, the cosensitized core/shell CdTe/Mn-CdS/ZnO NS shows a higher light absorbance ability in the entire region (curve f, Figure 2E) with absorption onset at 563 nm corresponding to a bandgap of 2.20 eV (curve f, Figure 2F). Introduction of ZnS layers within CdTe/Mn-CdS/ZnO NS gives the highest light absorption with absorption onset at 579 nm (2.14 eV). The ZnS layers may play a role as light scattering layers to increase the light absorption.

The higher light absorption ability results in a superior photoresponse performance. The photocurrent responses of these photoelectrodes are well consistent with their light absorption ability (Figure 2C and E). The photocurrent density also demonstrates a strong dependence on the structure. The core/shell CdTe/CdS/ZnO NS or CdTe/Mn-CdS/ZnO NS shows high photocurrent responses up to 4.06 and 4.98 mA/cm^2, respectively, dramatically higher than the values obtained with only one sensitizer. Here, A type II-like core−shell model is proposed to elucidate the possible charge transfer mechanism in CdTe/Mn-CdS/ZnO NS photoelectrode system (as describe in Scheme 1). In an ideal type II core/shell QD, the spatially separated electron and hole wave functions reduce their coulomb interaction, increasing the lifetimes of single and multiple exciton states. Meanwhile, shell-localized electrons and core-localized holes could achieve ultrafast electron transfer to adsorbed acceptors while simultaneously retarding the charge recombination process.[32] The subsequent Mn-CdS coating forms a layered shell on the core of CdTe QDs. When the cosensitized photoelectrode is brought into contact in a redox couple solution, the Fermi levels of semiconductors and the redox couple solution will be identical after electrostatic equilibrium. Such a Fermi level alignment causes upward and downward shifts of the band edges for CdTe QDs and CdS QDs, respectively. Therefore, a type II energy level alignment is formed. The elevated conduction band edge of CdTe QDs provides a higher driving force for the injection of photogenerated electrons from

Scheme 1. Band Diagram Schematic of the Photoelectrode and Mechanism of Photocatalysis Degradation

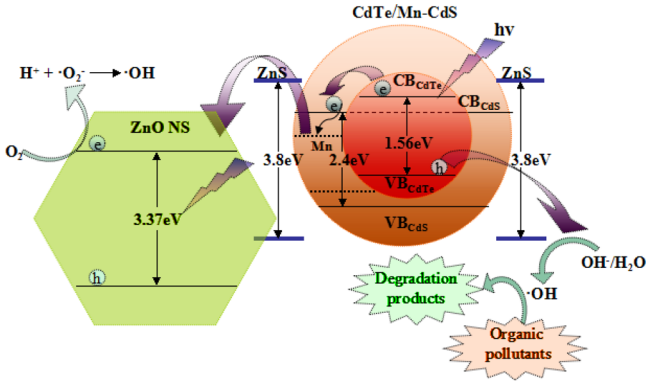

CdTe QDs to Mn-CdS shell, as well as the injection of excited holes.[20] Subsequently, the electrons are transferred to the Mn^4 T_1 state. The midgap states created by Mn doping cause electrons to get trapped and screen them from charge recombination with holes and oxidized polysulfide electrolyte.[33] Therefore, the spatial separation of electrons can be efficiently collected using an external circuit. This energy level alignment will be discussed in detail in the following work. Besides, the Mn-CdS coating layer, with band gap larger than that of CdTe and much lower oxidation potential, can provide a better coverage of the surface of CdTe QDs, resulting in low photooxidative degradation and surface defects. Thus, the Mn-CdS coating passivated the CdTe QDs surface and suppressed the charge recombination or the electron leakage to the electrolyte.[34] On the basis of the above experimental facts, we believe that the stepwise band-edge level, type-II structure core/shell CdTe/Mn-CdS sensitized photoelectrode, produces a leading role for the excellent photoelectrode performance (Scheme 1).[30,35]

Meanwhile, the d−d transition of Mn ($^4T_1$−$^6A_1$) is both spin and orbitally forbidden, resulting in a very long lifetime in the range of several hundreds of microseconds. Mn doped CdS QDs have been proved to be a powerful strategy to utilize long-lived charge carriers to boost the efficiency. So, Mn-CdS/ZnO NS photoelectrode displays a higher J_{sc} of 2.07 mA/cm^2 than that of CdS/ZnO NS (1.71 mA/cm^2).

The introduction of ZnS layers achieves the highest photocurrent density of 6.23 mA/cm^2. Ye et al.[36] reported the pioneer work on ZnS coating effect and pointed out that the ZnS pretreatment can passivate the surface states of ZnO NS and block the oxide surface to suppress the recombination at the interface between the oxide and sensitizers. The second ZnS

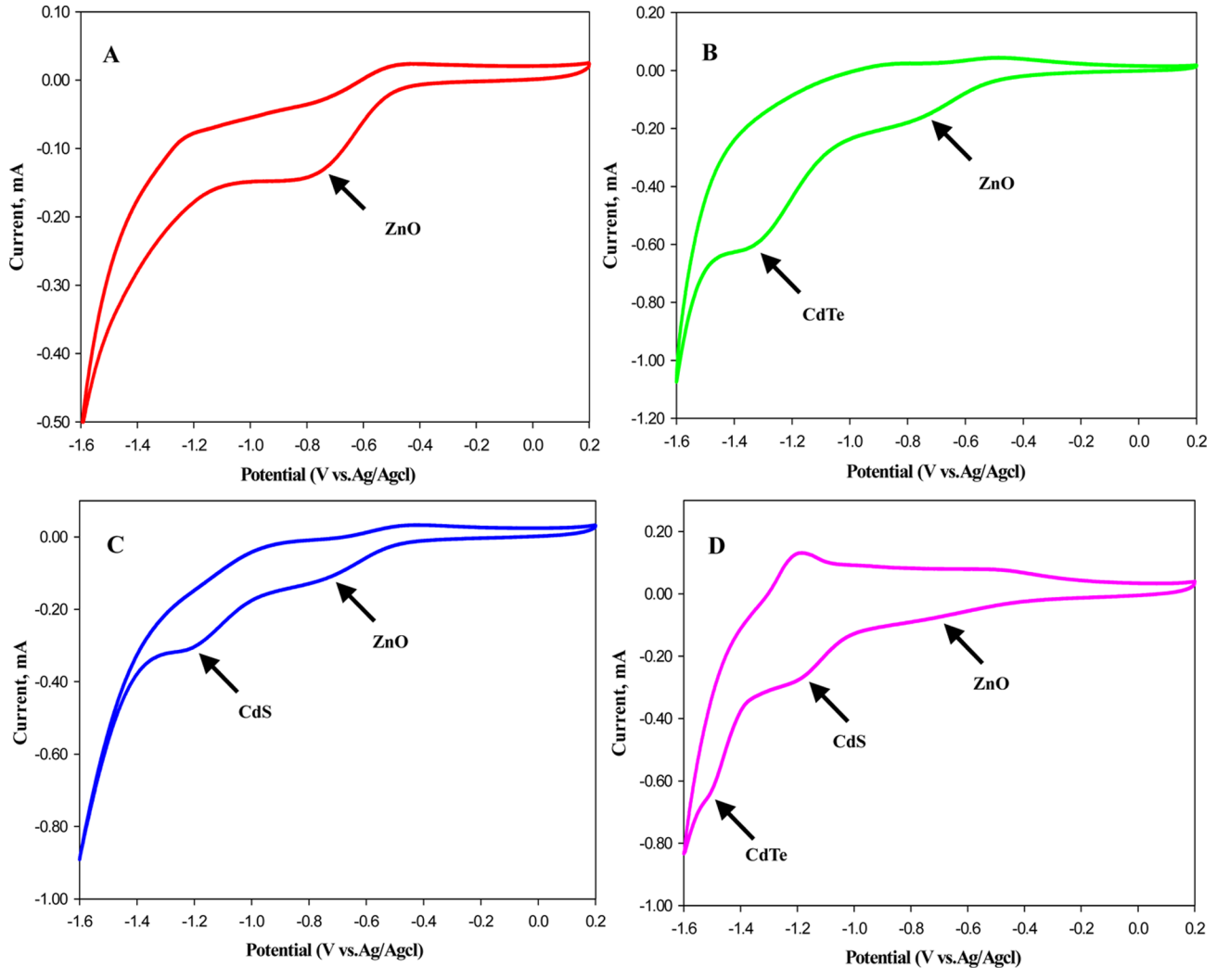

Figure 3. Cyclic voltammogram records of ZnO NS (A), CdTe/ZnO NS (B), CdS/ZnO NS (C), and CdTe/CdS/ZnO NS (D).

layer with a large bandgap at the electrode/electrolyte solution interfaces acted as a potential barrier, which was similar to an insulating layer employed in the conventional metal−insulator−semiconductor solar cells, allowing the adjustment of the electric field and potential distribution in the interface between the electrodes and the electrolyte and suppressing the dark current and back recombination of the injected electrons. As expected, ZnS/CdTe/Mn-CdS/ZnS/ZnO NS photoelectrode achieves the highest efficiency of 4.20% at −0.39 V vs Ag/AgCl as shown in Figure 2D.

Charge Transfer Mechanism of the Photoelectrode. Cyclic voltammetry (CV) is proposed to roughly elucidate the possible charge transfer mechanism, that is, to confirm the type II-like stepwise conduction band edge (as describe in Scheme 1). Figure 3A−D shows the CV records for ZnO NS, CdTe/ZnO NS, CdS/ZnO NS, and CdTe/CdS/ZnO NS, respectively. The energy levels of the conduction band edges can be calculated from the onset reduction potential (E^{red}) according to the following equations:[37]

$$E_{LUMO} = -E_a = -e(E^{red} + 4.71)\ \text{eV}$$

where the potential is measured relative to a Ag/AgCl reference electrode.

From Figure 3, one can see that the reduction potentials (conduction band edges) of CdTe and CdS are ca. −1.32 and −1.23 V corresponding to LUMO levels of −3.39 and −3.48 eV, respectively, while they exist in ZnO NS. While they form the core−shell structure in CdTe/CdS/ZnO NS, the reduction potentials of CdTe and CdS are shifted to −1.51 and −1.17 V, respectively, corresponding to LUMO levels of −3.2 and −3.54 eV. The conduction band edge of CdTe shifts upward, whereas that of CdS shifts downward. Changing the loading mass of CdS with different SILAR layers resulted in corresponding changes in reduction potential, while the potential of CdTe remains unchanged (Supporting Information Figure S3). These results clearly confirm a band structure reconfiguration of the core/shell CdTe/CdS/ZnO NS heterojunction, core/shell type II, which enables the quick separation of photogenerated electron−hole pairs, demonstrating a much more fluent electron transport.

Carrier Transfer and Recombination Behavior. To give a reasonable interpretation of the superior performance of the ZnS/CdTe/Mn-CdS/ZnS/ZnO NS photoelectrode, charge transport and recombination behavior were well investigated. The open-circuit dark−light−dark photovoltage response (Figure 4A) is conducted to further confirm the recombination kinetics of the photoelectrodes by monitoring the V_{oc} transient during relaxation from an illuminated quasi-equilibrium state to the dark equilibrium. Once the illumination is stopped, the accumulated electrons are slowly discharged by the recombination with holes trapped in the composite and dissolved oxygen in the electrolyte, which scavenges electrons. The photovoltage decay rate directly relates to the electron lifetime by the following expression:[20]

$$\tau_n = [-k_B T/e][dV_{oc}/d_t]^{-1}$$

where $k_B T$ is the thermal energy, e is the positive elementary charge, and dV_{oc}/d_t is the open-circuit voltage transient. Figure 4B is the plot of the response time obtained by applying this equation to the data in Figure 4A. At the same V_{oc} value, the response time of the photoelectrodes follows an order of ZnS/CdTe/Mn-CdS/ZnS/ZnO NS > CdTe/Mn-CdS/ZnO NS > CdTe/CdS/ZnO NS > Mn-CdS/ZnO NS ≈ CdTe/ZnO NS > CdS/ZnO NS > ZnO NS. As compared to CdTe, CdS are loose packed on the ZnO NS by SILAR deposition,[38] which will produce lots of recombination centers resulting in a shorter response time. After dopping CdS with Mn, the midgap states created by Mn cause electrons to get trapped and screen them from charge recombination with holes and oxidized polysulfide electrolyte.[33] So, the response time of the Mn-CdS/ZnO NS will be significantly improved and comparable to that of CdTe/ZnO NS. For the core/shell sensitizers, single and multiple exciton states lifetimes can be greatly increased by this novel structure; these carriers are efficiently collected by an external circuit through stepwise band-edge level (the type-II structure). So, the response times are larger than the single sensitizers. Similar, the Mn-CdS shell is also superior to the undoping CdS. Longer response times are obtained for ZnS/CdTe/Mn-CdS/ZnS/ZnO NS photoelectrode, indicating less recombination in this system, possibly because of the great suppression of the back recombination of the injected electron.

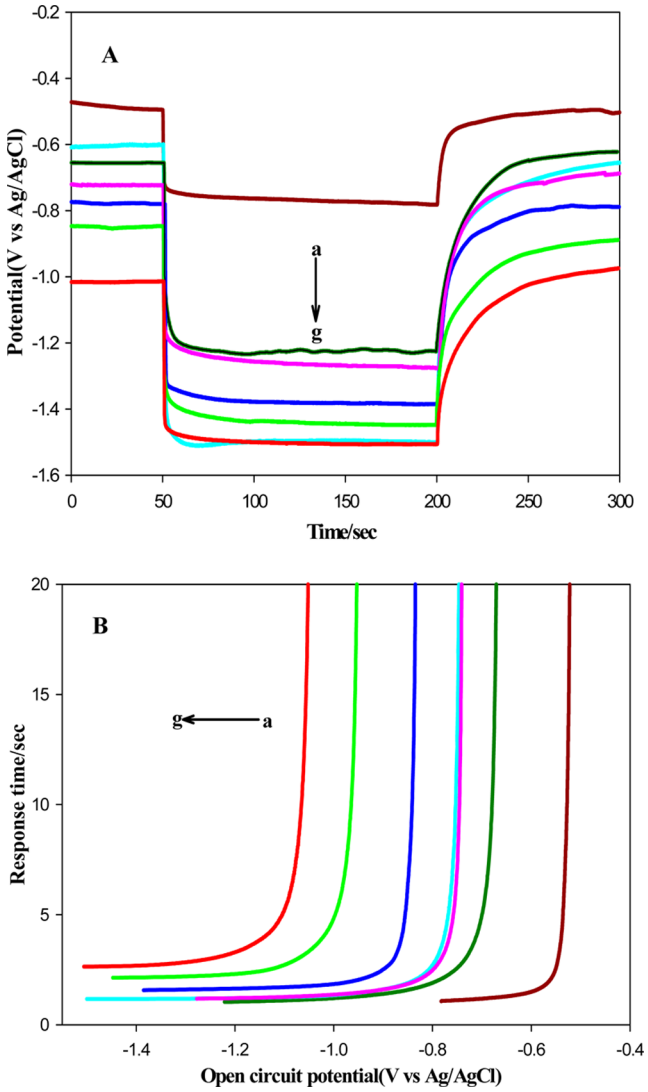

Figure 4. (A) The open-circuit photovoltage responses of a, ZnO NS; b, CdTe/ZnO NS; c, CdS/ZnO NS; d, Mn-CdS/ZnO NS; e, core/shell CdTe/CdS/ZnO NS; f, core/shell CdTe/Mn-CdS/ZnO NS; g, ZnS/CdTe/Mn-CdS/ZnS/ZnO NS. (B) Response time determined by open-circuit potential decay for corresponding photoelectrodes shown in (A).

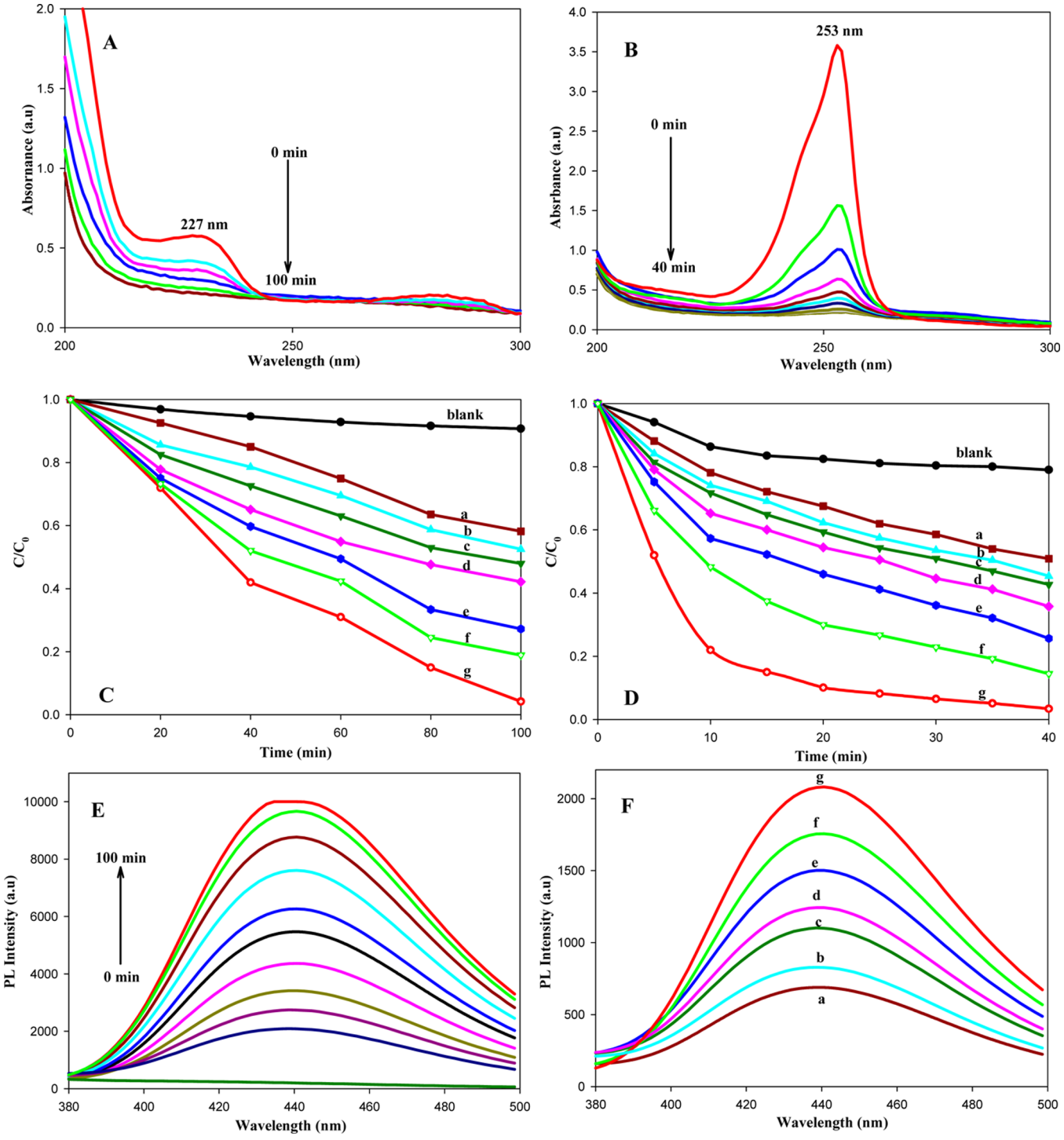

Figure 5. UV−vis determination of photoelectrocatalytic degradation of 20 mg/L 2,4-D (A) and 9-AnCOOH (B) using ZnS/CdTe/Mn-CdS/ZnS/ZnO NS photoelectrode under AM 1.5G illumination. (C,D) Corresponding photocatalytic performances of different photoelectrodes. L spectra measured during illumination with ZnS/CdTe/Mn-CdS/ZnS/ZnO NS (E) or different photoelectrodes (F). For all of the curves: a, ZnO NS; b, CdTe/ZnO NS; c, CdS/ZnO NS; d, Mn-CdS/ZnO NS; e, core/shell CdTe/CdS/ZnO NS; f, core/shell CdTe/Mn-CdS/ZnO NS; g, ZnS/CdTe/Mn-CdS/ZnS/ZnO NS. For (C) and (D), blank test was done without catalyst.

The recombination and transfer behavior of the photoinduced electrons and holes is further verified by emission spectra. As shown in Supporting Information Figure S4, curve a shows the emission peak at 553 nm of CdTe QDs on clean FTO substrate. When CdTe QDs are anchored onto ZnO NS substrate, the significant quenching of the emission peak is observed (curve b). Curve c displays the emission spectra of CdS/ZnO NS. After the CdTe/ZnO NS photoelectrode was coated with CdS QDs or Mn-CdS QDs, the hybrid nanostructure exhibited more obvious quenched emissions (curves d and e); this quenching behavior confirms the excited-state interaction among the semiconductors, indicating that most of the excited electrons in the photoelectrode were transferred to the ZnO NS substrate,

which significantly improved the photovoltaic performance of the system.

Photocatalytic Performance and Mechanism of the ZnS/CdTe/Mn-CdS/ZnS/ZnO NS. The photocatalytic performance of the ZnS/CdTe/Mn-CdS/ZnS/ZnO NS was evaluated by the photodegradation of 2,4-D and 9-AnCOOH under visible light, with the results shown in Figure 5. After 100 min illumination, all characteristic peaks of 2,4-D disappear completely, indicating that the 2,4-D is completely degraded, while 40 min illumination degrades 9-AnCOOH completely. Such a catalytic efficiency is satisfactory as compared to the previous research.[39,40] As illustrated in Figure 5C,D, it is clearly seen that under identical conditions, the ZnS/CdTe/Mn-CdS/ZnS/ZnO NS shows much higher activity than that of ZnO NS with other modifications. The degradation mechanism was elucidated on the basis of the reported ones[10,27] and is shown in Scheme 1 with the following equations:

$$\mathrm{CdTe/Mn\text{-}CdS} + h\nu \rightarrow \mathrm{CdTe}(h^+)/\mathrm{Mn\text{-}CdS}(e^-) \quad (1)$$

$$\mathrm{ZnO} + h\nu \rightarrow \mathrm{ZnO}(h^+ + e^-) \quad (2)$$

$$\mathrm{CdTe}(h^+)/\mathrm{Mn\text{-}CdS}(e^-) + \mathrm{ZnO}(h^+ + e^-) \rightarrow \mathrm{ZnO}(e^- + e^-) + \mathrm{CdTe}(h^+ + h^+)/\mathrm{Mn\text{-}CdS} \quad (3)$$

$$\mathrm{ZnO}(e^- + e^-) + \mathrm{O_2} \rightarrow \mathrm{ZnO} + \cdot\mathrm{O_2}^- \quad (4)$$

$$\cdot\mathrm{O_2}^- + \mathrm{H}^+ \rightarrow \mathrm{HOO}\cdot \rightarrow \rightarrow \cdot\mathrm{OH} \quad (5)$$

$$\mathrm{CdTe}(h^+ + h^+)/\mathrm{Mn\text{-}CdS} + \mathrm{H_2O} \rightarrow \mathrm{CdTe/Mn\text{-}CdS} + \cdot\mathrm{OH} + \mathrm{H}^+ \quad (6)$$

$$\mathrm{CdTe}(h^+ + h^+)/\mathrm{Mn\text{-}CdS} + \mathrm{OH}^- \rightarrow \mathrm{CdTe/Mn\text{-}CdS} + \cdot\mathrm{OH} \quad (7)$$

$$\cdot\mathrm{OH} + \text{organic pollutants} \rightarrow \text{degradation products} \quad (8)$$

Under illumination, electron−hole pairs are generated on CdTe/Mn-CdS QDs. The electrons are quickly transferred from CdTe/Mn-CdS QDs to the conduction band of ZnO NS. Once the electrons diffuse into the ZnO CB, the probability of its decay is small because there is little electronic backflow and little free holes in ZnO due to the existence of ZnS buffer layers. Electrons (e^-) accumulated on the surface of ZnO are scavenged by dissolved oxygen molecules to yield superoxide radical anion $\cdot O_2^-$, producing hydroxyl radical (·OH). Meanwhile, the holes generated on the valence band (VB) of CdTe/Mn-CdS QDs are not transferred to the corresponding band of ZnO due to the CdTe/Mn-CdS VB being more cathodic than that of ZnO. Holes in CdTe/Mn-CdS QDs can potentially react with water or OH^- adhering to the surface of the photoelectrode to form highly reactive hydroxyl radicals ·OH, a strong oxidizing agent to decompose the organic pollutants.

Hydroxyl radicals (·OH) generated on the surface of photocatalysts during the illumination are the main species responsible for the degradation of pollutant molecules. The formed ·OH was detected by the PL technique using TA as a probe molecule. TA readily reacts with ·OH to produce the highly fluorescent product, TAOH, which was proportional to the amount of ·OH. As shown in Figure 5E, the PL intensity increases gradually with increasing irradiation time with ZnS/CdTe/Mn-CdS/ZnS/ZnO NS as photocatalyst, indicating ·OH is indeed formed during this photocatalytic process. To illustrate photocatalytic properties of different photoelectrodes, the PL is recorded after irradiation 10 min, and the results are shown in Figure 5F. From ZnO NS (curve a) to ZnS/CdTe/Mn-CdS/ZnS/ZnO NS (curve g), the PL intensity shows a gradual increase. The results confirm the best photocatalytic performance of ZnS/CdTe/Mn-CdS/ZnS/ZnO NS.

The stability of the prepared catalyst was evaluated by repeatedly measuring its efficiency in photoelectrocatalytic degradation of 2,4-D and 9-AnCOOH. The degradation efficiency toward 2,4-D with 100 min illumination decreases from 100% on the first run to 95.8% on the fourth run (Supporting Information Figure S5A). The degradation efficiency toward 9-AnCOOH with 40 min illumination is 100% on the first run, and 96.6% on the fourth run (Supporting Information Figure S5B).

CONCLUSIONS

A multicomposite photoelectrode, ZnS/CdTe/Mn-CdS/ZnS/ZnO NS, was prepared using three-dimensional and macroporous ZnO NS as substrate. The charge transfer mechanism was investigated in detail. The photocurrent intensity of the ZnO NS was greatly enhanced by cosensitization with CdTe and Mn-CdS QDs, which formed a core/shell stepwise band-edge structure favoring the transport of excited electrons and holes across the composite. By introduction of the ZnS layers potential barrier, the CdTe/Mn-CdS/ZnO NS becomes more stable with the total energy conversion efficiency fundamentally improved. Meanwhile, photocatalytic performance of the prepared photoelectrode was investigated by photodegradation of organic pollutants. The photodegradation mechanism was proposed on the basis of band alignment to elucidate the enhancement of efficiency of ZnS/CdTe/Mn-CdS/ZnS/ZnO NS photocatalysts.

ASSOCIATED CONTENT

Supporting Information

SEM images of $Zn_5(OH)_8Cl_2{\cdot}H_2O$ and ZnO NS, nitrogen adsorption−desorption isotherms of ZnO NS, cyclic voltammogram records of CdTe/CdS/ZnO NS, and PL spectra of different photoelectrodes. Photoelectrocatalytic stability of ZnS/CdTe/Mn-CdS/ZnS/ZnO NS. This material is available free of charge via the Internet at http://pubs.acs.org.

AUTHOR INFORMATION

Corresponding Author

*Tel.: +8673188821848. E-mail: qycai0001@hnu.edu.cn.

Notes

The authors declare no competing financial interest.

ACKNOWLEDGMENTS

This work was financially supported by the National Basic Research Program of China (Grant no. 2009CB421601), the National Science Foundation of China (Grant nos. 21175038, 21235002), and the Hunan Provincial Innovation Foundation for Postgraduate.

REFERENCES

(1) Qiu, Y.; Yan, K.; Deng, H.; Yang, S. Secondary Branching and Nitrogen Doping of ZnO Nanotetrapods: Building a Highly Active Network for Photoelectrochemical Water Splitting. *Nano Lett.* **2012**, *12*, 407−413.

(2) Lopez, C. M.; Choi, K. S. Enhancement of Electrochemical and Photoelectrochemical Properties of Fibrous Zn and ZnO Electrodes. *Chem. Commun.* **2005**, 3328−3330.

(3) Law, M.; Greene, L. E.; Johnson, J. C.; Saykally, R.; Yang, P. D. Nanowire Dye-Sensitized Solar Cells. *Nat. Mater.* **2005**, *4*, 455−459.
(4) Mor, G. K.; Shankar, K.; Paulose, M.; Varghese, O. K.; Grimes, C. A. Use of Highly-Ordered TiO_2 Nanotube Arrays in Dye-Sensitized Solar Cells. *Nano Lett.* **2006**, *6*, 215−218.
(5) Singh, N.; Mehra, R. M.; Kapoor, A.; Soga, T. ZnO Based Quantum Dot Sensitized Solar Cell using CdS Quantum Dots. *J. Renewable Sustainable Energy* **2012**, *4*, 013110.
(6) Chen, H. N.; Li, W. P.; Liu, H. C.; Zhu, L. Q. CdS Quantum Dots Sensitized Single-and Multi-Layer Porous ZnO Nanosheets for Quantum Dots-Sensitized Solar Cells. *Electrochem. Commun.* **2011**, *13*, 331−334.
(7) Tak, Y.; Hong, S. J.; Lee, J. S.; Yong, K. Fabrication of ZnO/CdS Core/Shell Nanowire Arrays for Efficient Solar Energy Conversion. *J. Mater. Chem.* **2009**, *19*, 5945−5951.
(8) Leschkies, K. S.; Divakar, R.; Basu, J.; Enache-Pommer, E.; Boercker, J. E.; Carter, C. B.; Kortshagen, U. R.; Norris, D. J.; Aydil, E. S. Photosensitization of ZnO Nanowires with CdSe Quantum Dots for Photovoltaic Devices. *Nano Lett.* **2007**, *7*, 1793−1798.
(9) Emin, S.; Fanetti, M.; Abdi, F. F.; Lisjak, D.; Valant, M.; Krol, R. V. D.; Dam, B. Photoelectrochemical Properties of Cadmium Chalcogenide Sensitized Textured Porous Zinc Oxide Plate Electrodes. *ACS Appl. Mater. Interfaces* **2013**, *5*, 1113−1121.
(10) Liu, D. Q.; Zheng, Z. Z.; Wang, C. Q.; Yin, Y. Q.; Liu, S. Q.; Yang, B.; Jiang, Z. H. CdTe Quantum Dots Encapsulated ZnO Nanorods for Highly Efficient Photoelectrochemical Degradation of Phenols. *J. Phys. Chem. C* **2013**, *117*, 26529−26537.
(11) Wang, G. M.; Yang, X. Y.; Qian, F.; Zhang, J. Z.; Li, Y. Double-Sided CdS and CdSe Quantum Dot Co-Sensitized ZnO Nanowire Arrays for Photoelectrochemical Hydrogen Generation. *Nano Lett.* **2010**, *10*, 1088−1092.
(12) Bai, Y.; Yu, H.; Li, Z.; Amal, R.; Lu, G. Q.; Wang, L. Z. In Situ Growth of a ZnO Nanowire Network within a TiO_2 Nanoparticle Film for Enhanced Dye-Sensitized Solar Cell Performance. *Adv. Mater.* **2012**, *24*, 5850−5856.
(13) Fu, M.; Zhou, J.; Xiao, Q.; Li, B.; Zong, R.; Chen, W.; Zhang, J. ZnO Nanosheets with Ordered Pore Periodicity via Colloidal Crystal Template Assisted Electrochemical Deposition. *Adv. Mater.* **2006**, *18*, 1001−1004.
(14) Wang, H.; Wang, T.; Wang, X.; Liu, R.; Wang, B.; Wang, H.; Xu, Y.; Zhang, J.; Duan, J. Double-Shelled ZnO/CdSe/CdTe Nanocable Arrays for Photovoltaic Applications: Microstructure Evolution and Interfacial Energy Alignment. *J. Mater. Chem.* **2012**, *22*, 12532−12537.
(15) Jin, M. J.; Chen, X. Y.; Gao, Z. M.; Ling, T.; Du, X. W. Improve Photo-Electron Conversion Efficiency of ZnO/CdS Coaxial Nanorods by P-Type CdTe Coating. *Nanotechnology* **2012**, *23*, 485401−485409.
(16) Rawal, S. B.; Sung, S. D.; Moon, S. Y.; Shin, Y. J.; Lee, W. I. Optimization of CdS Layer on ZnO Nanorod Arrays for Efficient CdS/CdSe Co-Sensitized Solar Cell. *Mater. Lett.* **2012**, *82*, 240−243.
(17) Chou, C. Y.; Li, C. T.; Lee, C. P.; Lin, L. Y.; Yeh, M. H.; Vittal, R.; Ho, K. C. ZnO Nanowire/Nanoparticles Composite Films for the Photoanodes of Quantum Dot-Sensitized Solar Cells. *Electrochim. Acta* **2013**, *88*, 35−43.
(18) Tian, J. J.; Lv, L. L.; Wang, X. Y.; Fei, C. B.; Liu, X. G.; Zhao, Z. X.; Wang, Y. J.; Cao, G. Z. Microsphere Light-Scattering Layer Assembled by ZnO Nanosheets for the Construction of High Efficiency (>5%) Quantum Dots Sensitized Solar Cells. *J. Phys. Chem. C* **2014**, DOI: 10.1021/jp412525k.
(19) Gao, X. F.; Li, H. B.; Sun, W. T.; Chen, Q.; Tang, F. Q.; Peng, L. M. CdTe Quantum Dots-Sensitized TiO_2 Nanotube Array Photoelectrodes. *J. Phys. Chem. C* **2009**, *113*, 7531−7535.
(20) Sheng, P. T.; Li, W. L.; Cai, J.; Wang, X.; Tong, X.; Cai, Q. Y.; Grimes, C. A. A Novel Method for Preparation of Photocorrosion Stable Core/Shell CdTe/CdS Quantum Dot TiO_2 Nanotube Array Photoelectrode Demonstrating an AM 1.5G Photoconversion Efficiency of 6.12%. *J. Mater. Chem. A* **2013**, *1*, 7806−7815.
(21) Norris, D. J.; Efros, A. L.; Erwin, S. C. Doped Nanocrystals. *Science* **2008**, *319*, 1776−1779.
(22) Karan, N. S.; Sarma, D. D.; Kadam, R. M.; Pradhan, N. Doping Transition Metal (Mn or Cu) Ions in Semiconductor Nanocrystals. *J. Phys. Chem. Lett.* **2010**, *1*, 2863−2866.
(23) Santra, P. K.; Kamat, P. V. Mn-Doped Quantum Dot Sensitized Solar Cells: A Strategy to Boost Efficiency over 5%. *J. Am. Chem. Soc.* **2012**, *134*, 2508−2511.
(24) Yang, S. M.; Huang, C. H.; Zhai, J.; Wang, Z. S.; Jiang, L. High Photostability and Quantum Yield of Nanoporous TiO_2 Thin Film Electrodes Co-Sensitized With Capped Sulfides. *J. Mater. Chem.* **2002**, *12*, 1459−1464.
(25) Lee, H.; Bang, J.; Park, J.; Kim, S.; Park, S. Multilayered Semiconductor (CdS/CdSe/ZnS)-Sensitized TiO_2 Mesoporous Solar Cells: All Prepared by Successive Ionic Layer Adsorption and Reaction Processes. *Chem. Mater.* **2010**, *22*, 5636−5643.
(26) Qiu, J. H.; Guo, M.; Wang, X. D. Electrodeposition of Hierarchical ZnO Nanorod-nanosheet Structures and Their Applications in Dye-Sensitized Solar Cells. *ACS Appl. Mater. Interfaces* **2011**, *3*, 2358−2367.
(27) Khanchandani, S.; Kundu, S.; Patra, A.; Ganguli, A. K. Shell Thickness Dependent Photocatalytic Properties of ZnO/CdS Core-Shell Nanorods. *J. Phys. Chem. C* **2012**, *116*, 23653−23662.
(28) Xu, F.; Zhang, P.; Navrotsky, A.; Yuan, Z. Y.; Ren, T. Z.; Halasa, M.; Su, B. L. Hierarchically Assembled Porous ZnO Nanoparticles: Synthesis, Surface Energy, and Photocatalytic Activity. *Chem. Mater.* **2007**, *19*, 5680−5686.
(29) Hou, Q.; Zhu, L. Q.; Chen, H. N.; Liu, H. C.; Li, W. P. Highly Regular and Ultra-Thin Porous ZnO Nanosheets: An Indirect Electrodeposition Method Using Acetate-Containing Precursor and their Application in Quantum Dots-Sensitized Solar Cells. *Electrochim. Acta* **2013**, *94*, 72−79.
(30) Song, X.; Fu, Y. S.; Xie, Y.; Song, J. G.; Wang, H. L.; Sun, J.; Du, X. W. The Effect of Post-Annealing on the Conversion Efficiency of Solar Cells Sensitized by CdS Quantum Dots. *Semicond. Sci. Technol.* **2010**, *25*, 045031.
(31) Baskoutas, S.; Terzis, A. F. Size-Dependent Band Gap of Colloidal Quantum Dots. *J. Appl. Phys.* **2006**, *99*, 013708.
(32) Zhu, H. M.; Song, N. H.; Lian, T. Q. Wave Function Engineering for Ultrafast Charge Separation and Slow Charge Recombination in Type II Core/Shell Quantum Dots. *J. Am. Chem. Soc.* **2011**, *133*, 8762−8771.
(33) Hu, X.; Zhang, Q. X.; Huang, X. M.; Li, D. M.; Luo, Y. H.; Meng, Q. B. Aqueous Colloidal $CuInS_2$ for Quantum Dot Sensitized Solar Cells. *J. Mater. Chem.* **2011**, *21*, 15903−15905.
(34) Smith, A. M.; Nie, S. Semiconductor Nanocrystals: Structure, Properties, and Band Gap Engineering. *Acc. Chem. Res.* **2010**, *43*, 190−200.
(35) Luo, J. H.; Wei, H. Y.; Huang, Q. L.; Hu, X.; Zhao, H. F.; Yu, R. C.; Li, D. M.; Luo, Y. H.; Meng, Q. B. Highly Efficient Core-Shell $CuInS_2$-Mn Doped CdS Quantum Dot Sensitized Solar Cells. *Chem. Commun.* **2013**, *49*, 3881−3883.
(36) Xu, G. P.; Ji, S. L.; Miao, C. H.; Liu, G. D.; Ye, C. H. Effect of ZnS and CdS Coating on the Photovoltaic Properties of $CuInS_2$-Sensitized Photoelectrodes. *J. Mater. Chem.* **2012**, *22*, 4890−4896.
(37) Yang, Y.; Zhong, H. Z.; Bai, Z. L.; Zou, B. S.; Li, Y. F.; Scholes, G. D. Transition from Photoconductivity to Photovoltaic Effect in P3HT/$CuInSe_2$ Composites. *J. Phys. Chem. C* **2012**, *116*, 7280−7286.
(38) Li, T. L.; Lee, Y. L.; Teng, H. High-Performance Quantum Dot-Sensitized Solar Cells Based on Sensitization with $CuInS_2$ Quantum Dots/CdS Heterostructure. Energ. *Environ. Sci.* **2012**, *5*, 5315−5324.
(39) Tran, T. T. T.; Sheng, P. T.; Huang, C. A.; Li, J. Z.; Chen, L.; Yuan, L. J.; Grimes, C. A.; Cai, Q. Y. Synthesis and Photocatalytic Application of Ternary Cu-Zn-S Nanoparticle-Sensitized TiO_2 Nanotube Arrays. *Chem. Eng. J.* **2012**, *210*, 425−431.
(40) Kang, Q.; Liu, S. H.; Yang, L. X.; Cai, Q. Y.; Grimes, C. A. Fabrication of PbS Nanoparticle-Sensitized TiO_2 Nanotube Arrays and their Photoelectrochemical Properties. *ACS Appl. Mater. Interfaces* **2011**, *3*, 746−749.